International Journal of Geo-Information

MDPI

Article

Dynamic Monitoring of Agricultural Fires in China from 2010 to 2014 Using MODIS and GlobeLand30 Data

Huan Xie *, Li Du, Sicong Liu, Lei Chen, Sa Gao, Shuang Liu, Haiyan Pan and Xiaohua Tong

College of Surveying and Geo-informatics, Tongji University, 1239 Siping Road, Shanghai 200092, China; 0407duli@tongji.edu.cn (L.D.); sicong.liu@tongji.edu.cn (S.L.); 103495chen@tongji.edu.cn (L.C.); 1410900@tongji.edu.cn (S.G.); shushuangliu@163.com (S.L.); hypan@tongji.edu.cn (H.P.); xhtong@tongji.edu.cn (X.T.)

* Correspondence: huanxie@tongji.edu.cn; Tel.: +86-216-598-8851

Academic Editors: Songnian Li, Jun Chen, Shu Peng and Wolfgang Kainz

Received: 6 July 2016; Accepted: 21 September 2016; Published: 25 September 2016

Abstract: In the summer and autumn, which is the primary cropland planting preparation and harvest time, cropland burning is very common in China. The Moderate Resolution Imaging Spectroradiometer (MODIS) Terra active fire product (MOD14) and GlobeLand30-2010 data are used here to analyze the fire activity of the predominant land cover types. A total of 44,852 scenes of MOD14 images and MOD03 images are used, covering the whole of China from 20 May to 31 October during 2010 to 2014. Agricultural burning is a significant contributor to fire activity in China, and accounts for 60% on average of all the fire activity over the last five years. The spatial and temporal distribution of agricultural burning in seven different geographical regions is analyzed in detail. The experiments showed that the Central and Eastern China regions are the largest contributors to agricultural burning, producing 59%–80% of all the agricultural fires. At the national scale, the number of agricultural fire counts peak in June, which is associated primarily with winter burning of wheat croplands.

Keywords: MODIS; GlobeLand30 land cover data; agricultural fire

1. Introduction

Biomass burning is an important global emission source [1], and it has significant impacts on air quality, climate change, and human health [2]. Agricultural burning has been identified as the fourth largest type of biomass burning [3]. Crop residues are burned for a number of reasons, including clearing the crop residue, providing short-lived ash fertilization, and managing pests [4]. It is therefore normal practice that crop straw is burned in fields after harvest, especially in agricultural countries such as the USA, India, and China [5–7]. In recent years, farmland straw burning has been recognized as the main source of local air pollution in China, and has become the focus of public attention in both summer and autumn. The Chinese government has put forward a series of policies to ban the direct burning of crop straw in fields. However, the phenomenon of crop burning is still common in fields after harvest. Agricultural residue fires are generally smaller in size, less intense in strength, and shorter in duration than forest and savanna fires [8,9]. It is, however, difficult to monitor because of the scattered distribution of the crop burning and random burning time. To date, satellite remote sensing has provided effective approaches to monitor the occurrence and timing of fires over large areas at locations where field data are not available [10]. Remote sensing satellite data sets have been used for more than 20 years to monitor global fires [11,12]. Long-term monitoring of fires can help to characterize air pollution episodes caused by biomass burning over diverse spatial and temporal scales [13,14]. The Moderate Resolution Imaging Spectroradiometer (MODIS) onboard the Terra (1999)

and Aqua (2002) satellites was designed for the observation of actively burning fires and aerosol loading twice per day under relatively cloud-free conditions [15], resulting in it becoming a useful remote sensing data source for the monitoring of crop burning. The classification product of China's 30-m global land cover data (GlobeLand30-2010) provides the latest land-surface coverage data from 2010, which can be used for a more accurate monitoring of crop burning.

Giglio [16] used the MODIS Climate Modeling Grid (CMG) fire products to analyze the global distribution of biomass burning during 2000 to 2005 and quantified the extent to which the Terra and Aqua MODIS fire data records were in agreement with respect to the seasonality of fire activity. For the first time, the global agricultural fire activity was assessed using MOD14 and MODIS 1 km land cover data sets (MOD12) from 2001 to 2003 [4]. McCarty [17] used MOD14 and two land cover data with different resolutions to analyze the distribution of different types of crops for regional and state-levels in the Southeastern United States. The relationships between the density of fire detections and the patterns of land cover and land use (LCLU) in the central USA was discussed in [18]. Agricultural burning in the USA has been the subject of great attention in past years in the satellite studies of burning. Different MODIS fire products (e.g., MODIS Climate Modeling Grid, MOD/MYD14A1, MOD14/MYD14) have been used to study the significant effects of agricultural fire activity on the atmospheric environment in mid-eastern China [9,19]. A number of studies have estimated crop burning emissions, but they have not analyzed the crop burning in detail at the national scale in China [15,19–21]; to the best of our knowledge, few studies have focused on Chinese agricultural fire regimes at a larger scale and over a longer time period. Further analysis of detailed fire activities and the effects of fires on the environment still need to be considered in China [9].

In this study, we use the daily MODIS Terra active fire product (MOD14) and the MODIS Geolocation product (MOD03) from 2010 to 2014, as well as GlobeLand30-2010 data, to analyze the different land cover fire activities in the 33 provinces of China. The spatial and temporal occurrence of agricultural burning in the seven different geographical regions is then analyzed in detail. Moreover, the restrictions of the MODIS data and the GlobeLand30-2010 data and some uncertain factors affecting these research results are discussed.

2. Study Area, Data Set, and Methods

2.1. Study Area

China is a large agricultural country where a large amount of crop straw production takes place. Agricultural burning in China significantly contributes to the biomass burning in Asia [22], and amounts to 3%–6% of the global agricultural fires [4]. In China, the croplands owned by each farmer are usually very limited in size. Therefore, approximately 100 farms are located in each MODIS fire pixel (1 km $\times$ 1 km), and each agricultural fire usually covers a small area. Some studies have shown that crop burning usually occurs in the summer and autumn harvest periods in China. Zha [14] noted that the number of agricultural fires has two distinct peaks, in June (61%–86%) and October (5%–14%), and Korontzi [4] revealed that the number of agricultural fires peaks in July and late September to October. Therefore, in this paper, we study agricultural straw burning from 20 May to the end of October from 2010 to 2014. The study area includes 33 provinces of China, not including the Nansha Islands. Spatially, China can be divided into seven geographical regions: Northeast (NE), Northwest (NW), Northern (N), Southwest (SW), Southern (S), Eastern (E), and Central (C) (Taiwan, Hong Kong, and Macau are not included). The seven geographical regions and the corresponding GlobeLand30-2010 land cover data are outlined in Figure 1.

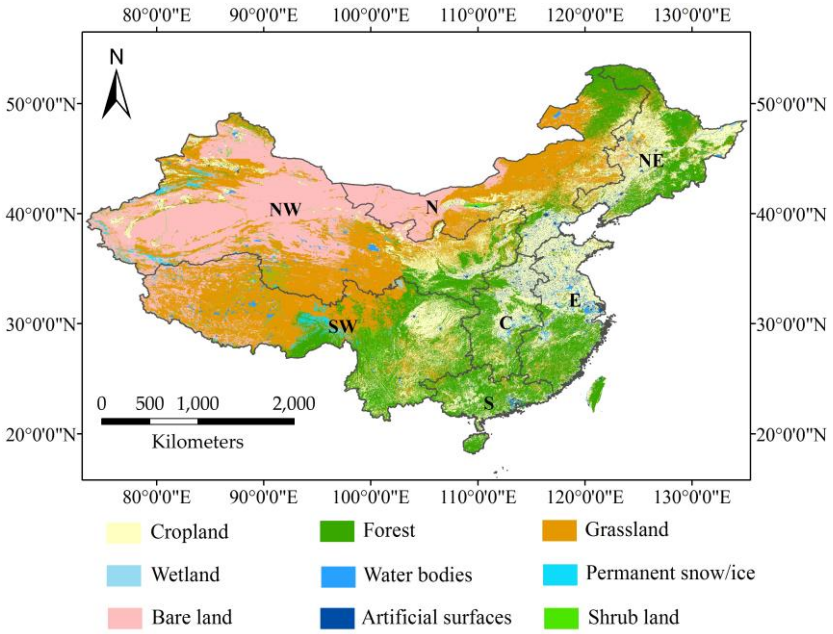

Figure 1. Map of the GlobeLand30-2010 land cover data in 33 provinces of China and the location of the seven geographical regions in this study.

2.2. MODIS Fire Activity Data

Some of the characteristics of MODIS data, such as the global coverage, the wide spectral range, and the high frequency of updates, mean that MODIS data are frequently used in the monitoring of fire activity. MOD14 is a part of the suite of global land-surface products [22], and has been producing data obtained by the Terra satellite since 2000 [11]. MOD14 monitors fire activity at a 1 km spatial resolution, with overpass times of approximately 10:30 AM and 10:30 PM local time [15,23]. The active fire algorithm (the Contextual Fire Detection Algorithm) uses multiple channels to detect thermal anomalies on a per-pixel basis, which in addition to fires, includes high-temperature point sources [10]. The fire detection strategy is based on absolute detection of the fire, if the fire is strong enough, and on detection relative to the thermal emission of surrounding pixels to detect weaker fires [10]. The fire detection algorithm of MOD14 product uses brightness temperatures derived from the MODIS 4 μm and 11 μm channels [10], denoted by T4 and T11, respectively. The thermal anomaly detection is achieved by setting several judgment thresholds (such as T4 and T4-T11) [10]. The confidence estimate, which ranges between 0% and 100%, is used to assign one of the three fire classes to all the fire pixels within the fire mask [24]. The MOD14 fire mask data set contains 10 levels of gray attribute values.

A total of 44,852 scenes of MOD14 images and MOD03 images were used in this study, covering the whole of China from 20 May to 31 October during 2010 to 2014. The amount of missing data is less than 10%, which is considered to be insignificant [4]. The missing dates are listed in Table 1.

2.3. GlobeLand30-2010 Land Cover Data

Table 1. Missing dates for the Terra MODIS land products from 2010 to 2014.

	Missing dates	
	Terra Day (~10:30 local time)	**Terra Night (~22:30 local time)**
2012	MOD14.A2012279 MOD14.A2012291 MOD14.A2012292	MOD14.A2012148 MOD14.A2012149 MOD14.A2012150 MOD14.A2012151 MOD14.A2012152
2013	MOD14.A2013288 MOD14.A2013290 MOD14.A2013297	MOD14.A2013292 MOD14.A2013283 MOD14.A2013297
2014	MOD14.A2014245 MOD14.A2014299 MOD14.A2014302	MOD14.A2014245 MOD14.A2014299 MOD14.A2014302

At the end of 2013, China successfully released the world's first 30 m resolution land cover data (GlobeLand30) products for the year of 2000 and 2010, which provide the comprehensive information and means needed for a wide range of surface coverage research. Eighteen institutions from seven ministries participated in the technology research and data production [25]. The classification images used in GlobeLand30-2010 are mainly Landsat TM, ETM+ in 2010 as a benchmark year, and HJ-1 satellite image set and the local region of BJ-1 satellite image set are complementary. According to the study period in this paper, we use the GlobeLand30 product from 2010 (GlobeLand30-2010) in this study. GlobeLand30-2010 includes 10 types of land cover, namely cropland, forest, grassland, shrub land, wetland, water bodies, tundra, artificial surfaces, bare land, and permanent snow/ice [26], which improves spatial resolution of the similar global land cover products by more than 10 times.To handle the classification process of 10 land cover types, a split-and-merge strategy was employed (i.e., first each class was identified in a prioritized sequence and then results were merged together) [26]. For the identification of each class, an approach based on the integration of pixel- and object-based methods with knowledge (POK-based) has been developed [26]. The method includes the pixel classification method, the object-oriented filtration, human-computer interaction inspection three steps, which gives full play to the advantages of classification algorithms and makes full use of all kinds of knowledge and experience to improve the quality of classification. This is a relatively new land cover data product of China, which features a higher precision. The two rank sampling spatial data model is used in the inspection of classification results. The first level is the map sample where the sampling unit is the map. The second level is the features sample where the sampling unit is the spatial classification elements in the sheet. By calculating the sample size needed to extract for sampling units in each level, the spatial variability analysis is used in combination with the rationally designed samples in order to verify the accuracy of the land cover classification using a considerable number of samples. It has been shown that the overall classification accuracy of GlobeLand30-2010 is better than 80%, and the kappa coefficient is around 0.75 [26].

2.4. Methods of Determining the Fire Points

In this study, after the preprocessing of the MOD14 data set and GlobeLand30-2010 data set, the MOD14 data set was combined with the GlobeLand30-2010 data set to obtain the distribution of fire activity within different land covers and credibility.

For MODIS Level1B and Level2 products, the HDF (Hierarchy Data Format) file typically contains latitude and longitude bands. In general, every MOD14 image corresponds to MODIS geolocation files (MOD03). As such, the geometric correction for MODIS image is carried out by using geo-location files built-in to the MODIS sensor. The IDL (Interface Description Language) of GLT (Geometry Lookup File)

algorithm was applied to conduct geometric correction of each scene MOD14 image. We then mosaic and clip the MOD14 images to obtain daily images of the study area from 2010 to 2014. According to the attributes of the MOD14 fire mask, we only extracted fire information with different confidence levels (with DN = 7, 8 and 9, corresponding to low, nominal, and high confidence level, respectively).

Fifty-two scenes of GlobeLand30-2010 images were used in the study. The GlobeLand30-2010 data sets was mosaicked and clipped to obtain the image of the study area. The GlobeLand30-2010 data of the study region (without the tundra land cover) are illustrated in Figure 1. In order to geometrically match the two different resolution data sets, we downsampled the GlobeLand30-2010 data and the cells were spatially aligned with the MOD14 pixels. Combining nine land cover types of GlobeLand30-2010 data, we used the grid calculator of daily MOD14 data and GlobeLand30-2010 data to classify the different fire confidence levels. Once we had the two aligned data sets, we first analyzed the temporal and spatial distribution of burning fires with different land cover types. Then, according to the scope of GlobeLand30-2010's cropland, the temporal and spatial distribution of agricultural fires were discussed in detail.

3. Spatial and Temporal Distributions of Fire Points

3.1. Overall Results

For these five years, a total of 19,854, 21,609, 30,842, 27,788, and 28,049 fire points (of all the confidence levels) were detected in 2010, 2011, 2012, 2013, and 2014 from the MODIS images, respectively. Low-confidence fire points accounted for 8.6% of the total over these five years (Table 2). In order to achieve the maximum fire detectability [18], all the confidence levels are considered in the following discussions. From the land cover data, over 95% of the fire points were located on cropland, forest, grassland, and artificial surfaces. Agricultural fires accounted for 55%–64% of the fires occurring in mainland China during the summer and autumn (see Figure 2).

Table 2. The proportion of agricultural fires and fires detected with low confidence levels.

	2010	2011	2012	2013	2014	Five-Year Total
Number of fire points	19,854	21,609	30,842	27,788	28,049	128,142
Percentage of fire points with a low confidence level	9.6%	7.8%	9.1%	8.1%	8.4%	8.6%
Number of agricultural fire points	10,488	11,227	18,958	15,239	16,523	72,435
Percentage of agricultural fire points with a low confidence level	9.7%	6.5%	8.5%	7.6%	7.2%	7.90%

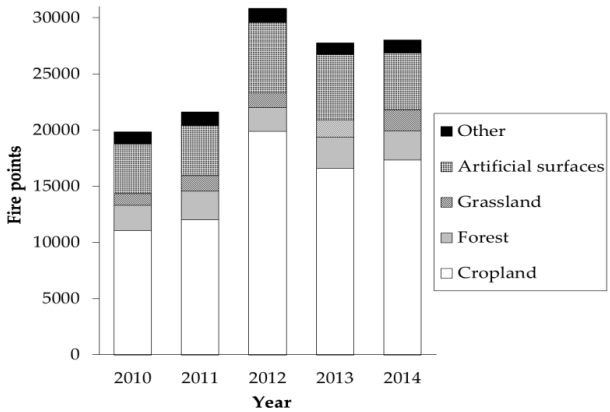

Figure 2. Fires in China occurring on the predominant land cover types from 2010 to 2014.

With regard to the spatial-temporal distribution of main land cover types of fire points from 2010 to 2014, we list the total amounts of each type of fire points for every month of each year in Figure 3 and the yearly spatial distribution of the different fires that occurred are shown in Figure 4. Each fire type has a unique spatiotemporal distribution, which is related to the different land-cover types. From Figure 3, we can see that the agricultural fire points and the artificial surface fire points (including industrial fires and residential fires) follow a fixed temporal pattern (see Figure 3a,c). The number of farmland burning fires peaked in June every year, and the average number reached 7742 among five years. In our study, the number of farmland burning fires was 13,023 in June 2012—over half of the average value. Meanwhile, the fires in forest and grassland land types are more random in their temporal distribution. The number of forest burning fires and grassland burning fires peaked in 2013 and 2014, respectively, as many as 2568, 1691. The spatial distributions of the agricultural fires and artificial surface fires are basically fixed (see Figure 4). Figure 4 shows something well known—that the majority of the grassland fires occurred in Eastern Inner Mongolia and Northeast and Southeast China, which to some extent reflects the credibility of the fire monitor in this article. The natural landscape can be roughly represented by the change from steppe to desert grassland from the east side to the west side in the north of China. Most of the forest burning fires were distributed in southern China, and some small burning clusters appeared in northeast China.

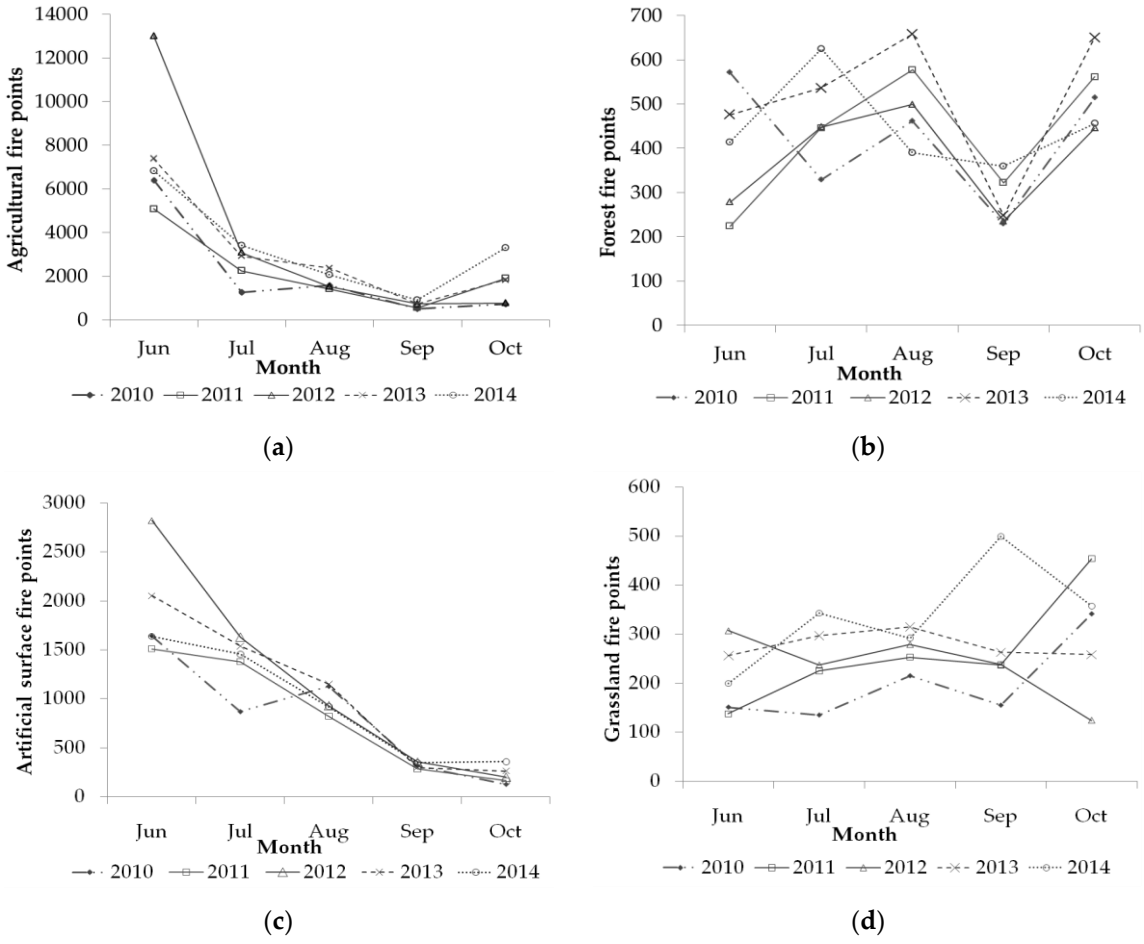

Figure 3. Monthly distribution of the fires in China within the predominant land cover types from 2010 to 2014: (**a**) agricultural fires; (**b**) forest fires; (**c**) artificial surface fires; (**d**) grassland fires.

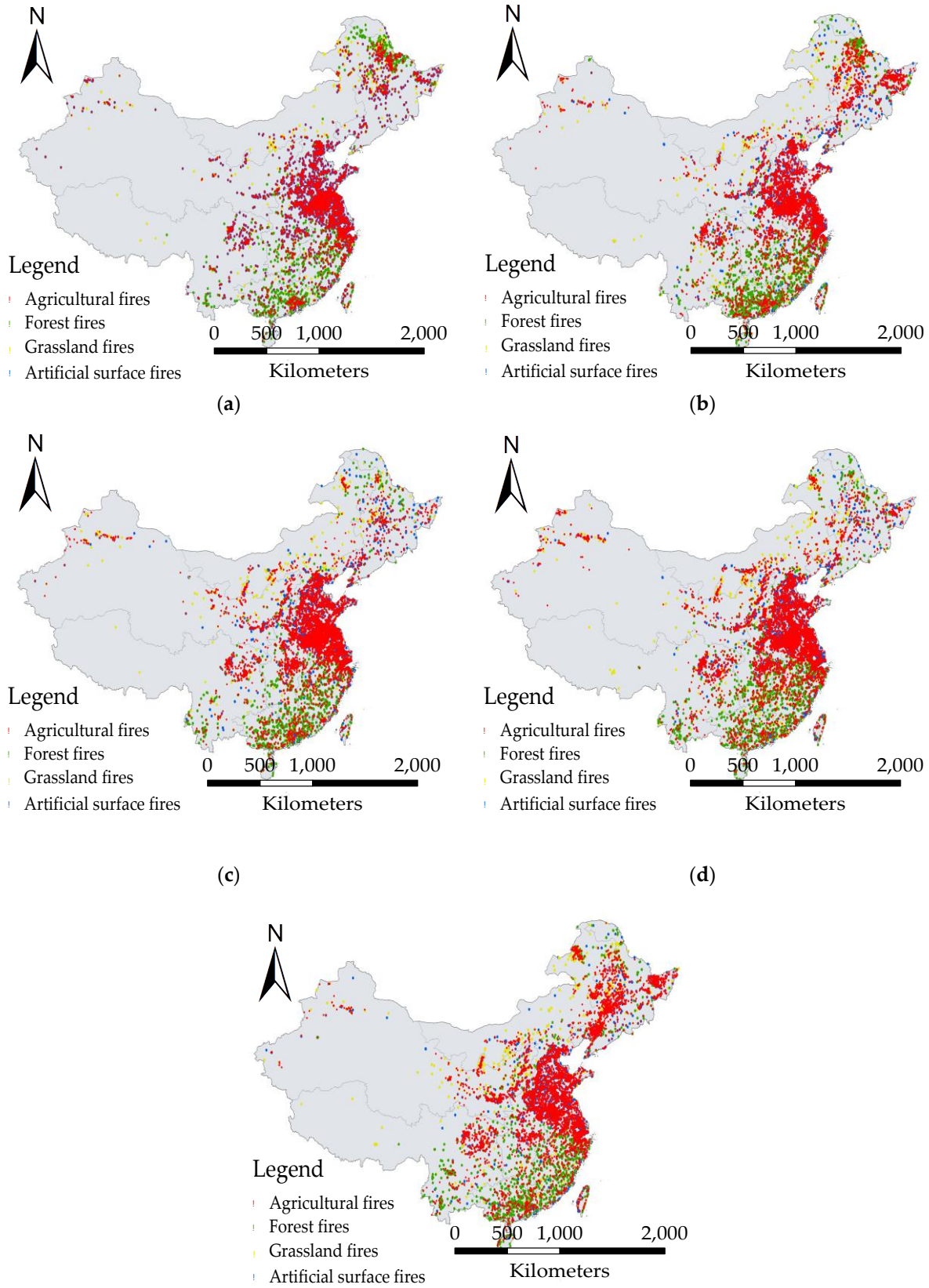

Figure 4. Spatial distribution of the main fires detected in China from 2010 to 2014: (**a**) 2010; (**b**) 2011; (**c**) 2012; (**d**) 2013; (**e**) 2014.

3.2. Agricultural Fires

The typical forms of cropland in GlobeLand30-2010 data mainly include arable land, cultivated land after harvested, paddy field in irrigation period, paddy field after the harvest, artificial grassland, arable land by land reclamation, and vegetable field [27]. The monitoring results from agricultural fires were obtained by cultivated land data of GlobeLand30-2010 and MOD14 data. The study found that the agricultural fires of China follow a fairly consistent pattern in space (Figure 4) and time (Figure 3a). There is a strong relationship between the location and timing of the burning, which is related to crop management, specifically harvesting and field preparation. The monthly average number of agricultural fire points detected in 2010, 2011, 2012, 2013, and 2014 is 7742, 2590, 1790, 689, and 1709, respectively. The number of agricultural fire counts peaked in June every year, reached the lowest levels in September, and then increased in October (Figure 3a). Figure 5 shows the daily variation in agricultural fires from 20 May to 30 June over the five years. Compared with the agricultural fires in late May and July, the number of agricultural fires was higher in June, and mainly comprised agricultural burning in the North China Plain region, where winter wheat is harvested in June. Figure 5 shows that agricultural fires were extremely common on 9 June and 13 June 2012, up to 2916 and 3989, respectively, which resulted in the agricultural fire points being higher than any other year in the June of 2012. Huang [21] used the MOD/MYD14A1 product and the Global Land Cover 2000 data base for China (GLC-China) data to investigate this phenomenon, which was found to be caused by the temperature and weather conditions.

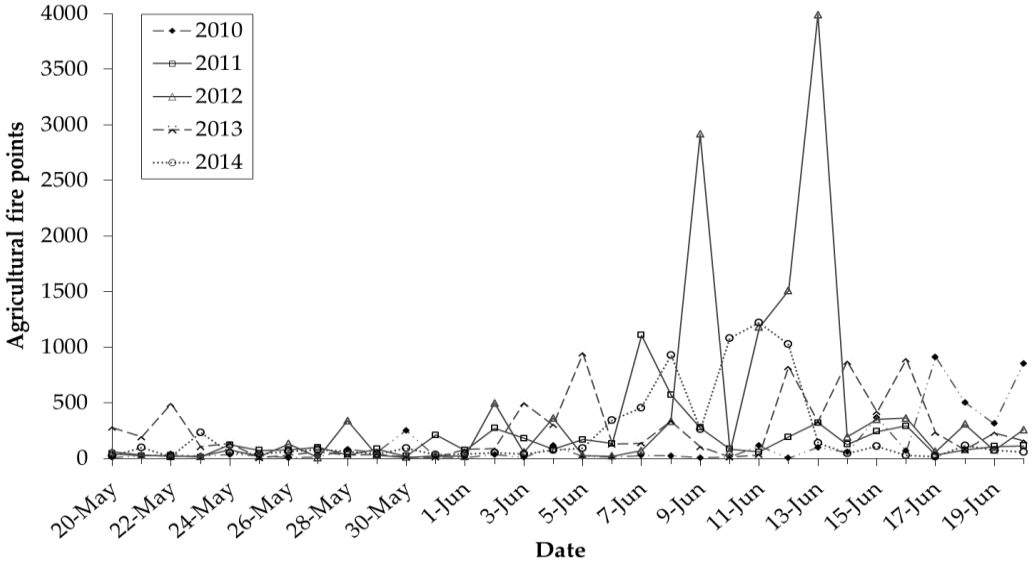

Figure 5. Daily variation in agricultural fires from 20 May to 20 June in China from 2010 to 2014.

According to the acquisition time of the MODIS data, we separated the agricultural fire points by day (Terra Day (~10:30 local time)) and night (Terra Night (~22:30 local time)). Figure 6 shows that the majority of the agricultural fires occurred in the daytime. The ratio in which the cropland burning happened in the daytime was 76%, 85%, 63%, 84%, and 81%, for each of the respective years of study. Figure 6 shows that cropland burning appeared on the night in 2012 is about 2–5 times more than other years. Reasons for agricultural burning occurring at night may be that the agricultural fire burned from early evening to night, or that the farmers burned the straw secretly at night to avoid detection. Xia [9] also mentioned that farmers often burn crop residue in the nighttime.

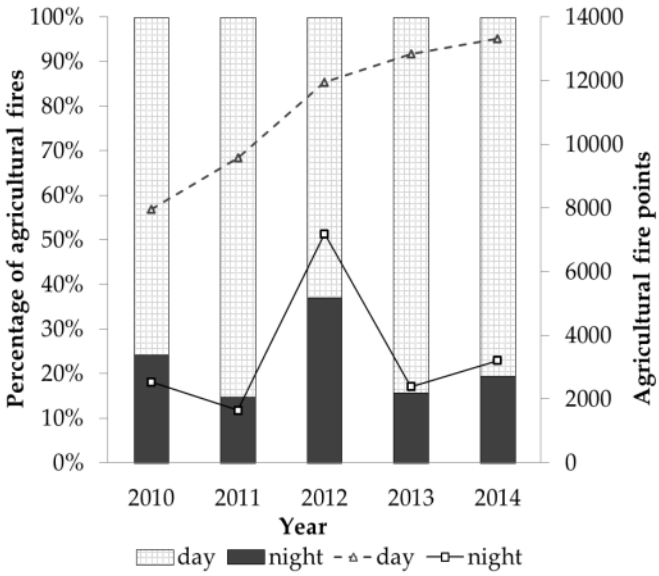

Figure 6. Interannual variations of the percentage of agricultural fires (stacked column chart) and the fire counts (line chart) at different times of the day.

Cropland burning does not show an even spatial distribution during the summer and autumn harvest periods (Figure 7). The summer harvest period in China is from late May to July, and the autumn harvest period is from late September to early November [14]. Figure 7 shows the spatial distribution of monthly agricultural fires from 2010 to 2014. Crop burning mainly occurred in Central and Eastern China, and large regions of fires were concentrated in the North China Plain during the summer harvest period. The number of agricultural fire points on 22 May to 31 July is 55,959 and on 1 August to 30 October is 20,948. Compared with the summer period, the number of agricultural fires was significantly reduced during the autumn period. The agricultural fire count increased in Northeast China in October, and several spatial clusters of agricultural fire detection appeared.

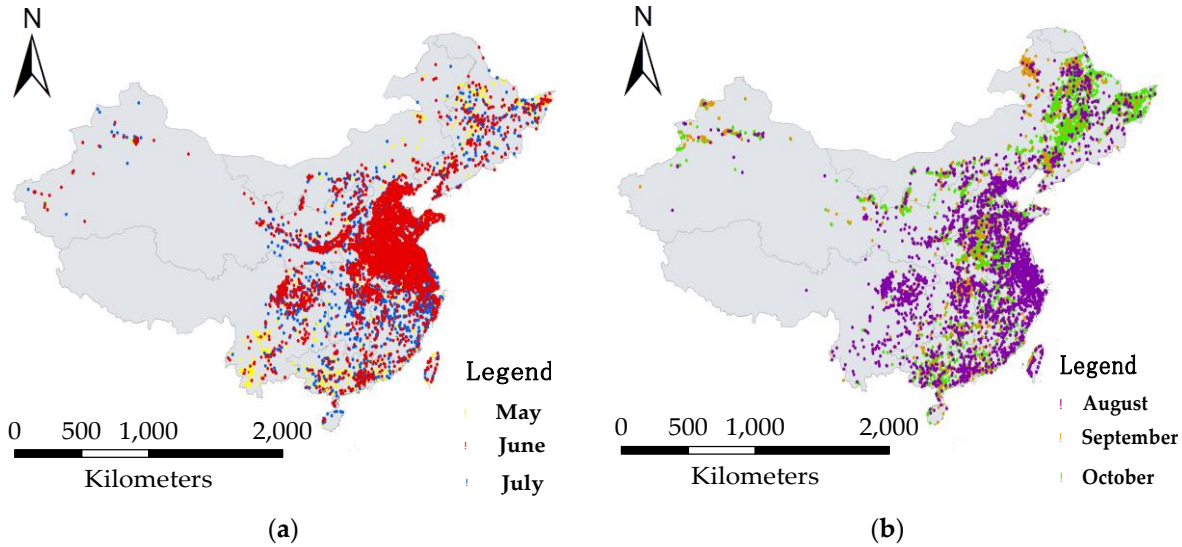

Figure 7. The spatial-temporal distribution of agricultural fires from 2010 to 2014: (**a**) May–July (summer harvest period); (**b**) August–October (autumn harvest period).

4. Discussions

4.1. The Regional Discussions of Agricultural Fires

Spatially, the study area can be divided into seven geographical regions. The monthly time series of the agricultural fires in the seven geographical regions is presented in Figure 8. The agricultural fires category has its own set of trends in each region across different seasons. The temporal and spatial distributions of agricultural fires in each region have been carried out based on the detailed analysis and discussion.

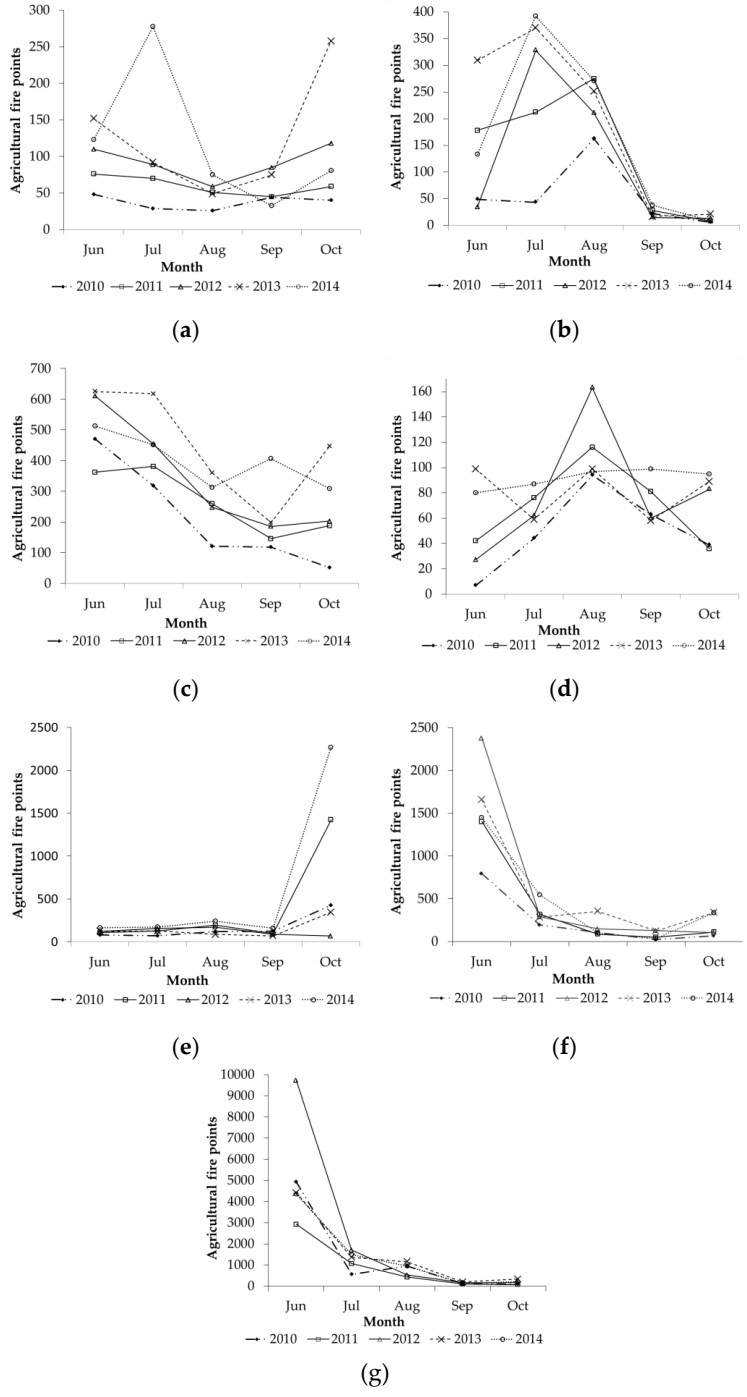

Figure 8. The monthly time series of agricultural fire detection in each region: (**a**) Northwest; (**b**) Southwest; (**c**) North China; (**d**) South China; (**e**) Northeast; (**f**) Central China; (**g**) Eastern China.

In the Northwest and Southwest regions, agricultural fires accounted for 5.3%, 8.9%, 5.7%, 11%, and 9% of all the fires in 2010, 2011, 2012, 2013, and 2014, respectively. In the Northwest region, where the major crops are wheat, cotton, and corn, agricultural fires were mainly localized in northwest Xinjiang, north-central Gansu, central Shaanxi, and northern Ningxia. Figure 8a shows that cropland burning was unusually active in October 2013 and July 2014. The agricultural fires in 2013 accounted for 45% of all fires in the Xinjiang region for five years. Agricultural fires in 2014 accounted for 42% of all fires in Shanxi during 2010 to 2014. Figure 8 shows that cropland burning fires in the Southwest region were mainly concentrated in July and August, up to 74%. Agricultural fires in the Southwest region, where rice and corn is mainly planted, mainly occurred in Sichuan and Chongqing during the summer and autumn seasons. The Sichuan Basin and Yunnan-Guizhou Plateau are important rice producing areas in China. The proportions of agricultural fires were higher than the other years in 2011 and 2013 because of the large number of fires in Sichuan and Guizhou (Figure 9).

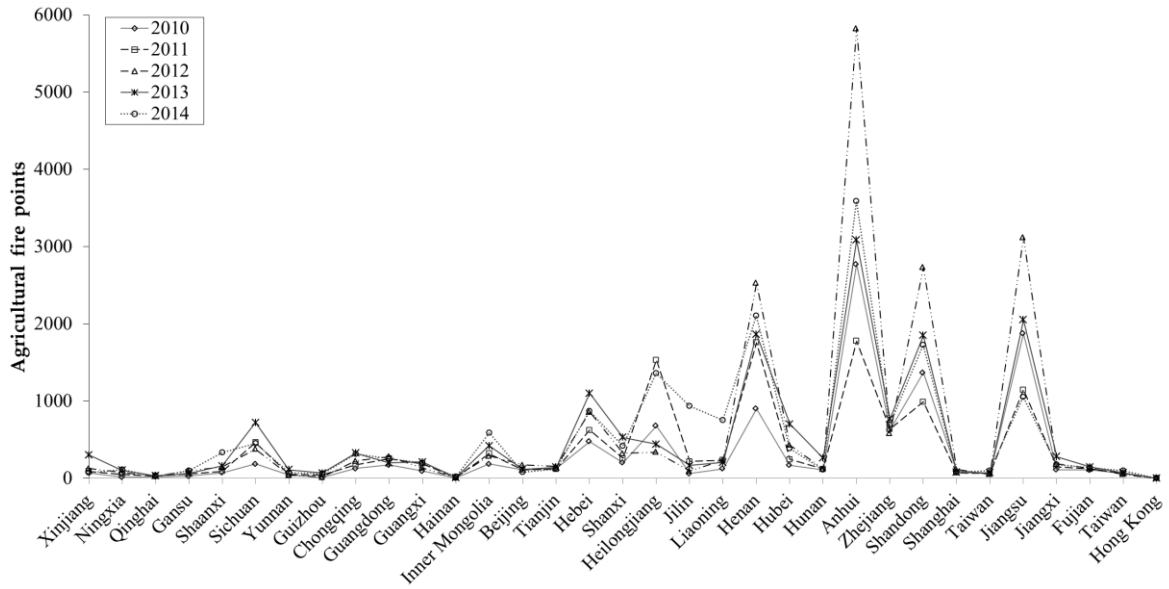

Figure 9. Spatial distribution of agricultural fires at a provincial level from 2010 to 2014.

The North China region contributed to an average of 12% of all the agricultural burning detected in China, and it was the third largest contributor to agricultural burning. Agricultural burning in North China was concentrated in Hebei and accounted for 76% of all agricultural fires in the region; this is likely because the province has a relatively large cultivation area, and the prohibition of crop straw burning is less strict than in Beijing and Tianjin. Agricultural burning in this region was mainly concentrated in the summer season, with June and July accounting for 57% of the number of agricultural fires, likely because this is when the harvest of the wheat and rapeseed occurs in the region. This phenomenon is consistent with the local sowing and harvest times.

The multiple-cropping rice, winter wheat, and winter rapeseed are mainly cultivated in South China. As shown in Figure 8d, a peak appeared in August which was related to the harvesting of early-season rice [28]. The low proportion of agricultural fires in Guangxi in 2012 led to a decreased proportion in South China for this year (Figure 9). This region is located in the tropics, with abundant water and sunshine, and has two or even three harvests each year. However, cropland burning is not a notable occurrence in the region during the summer and autumn. The Northeastern region is located in a high latitude area, and has just one harvest in the whole year, and its main crops are spring maize, spring wheat, rice, and beans. Agricultural fires accounted, on average, for 11% of all the fires detected in the region of Northeastern China. The percentage of agricultural fires in Heilongjiang exceeded the average of the other years by 6% in 2011. The maximum fire activity in 2010, 2011, 2013, and 2014

in this region occurred in October, which is in agreement with agricultural practices. In this region, spring maize, spring wheat, and rice are sown in late April, and the sowing time for beans is mid-May. Early October is the main harvest season for almost all the crops [28]. The agricultural fires in October 2012 only contributed 1.5% for the year's agricultural burning in the region, which can be primarily attributed to adverse weather conditions (i.e., the increased precipitation affected the farmland straw burning in October 2012 [29]).

Central China and Eastern China are the main agricultural zones. There are suitable climatic conditions for agricultural production in the region, and, as such, the region accounts for almost half of the country's agricultural production [21]. Extensive agricultural fires occurred in the region and accounted for 59%–80% of all the fires. Wheat and maize are the primary crops because of the widespread use of the wheat-maize rotation system in the area [28]. In the region, the agricultural fires burning peak occurred in the summer season each year. We detected that agricultural fires in June accounted for 73%, 66%, 79%, 59%, and 60% of all fires during 2010 to 2014 in the zones, which is related to the burning of winter wheat and the clearing of cropland for summer maize cultivation. Winter wheat is sown in mid-October and harvested at the end of May. Summer maize is sowed in mid-June and harvested at the end of September. Figure 8f,g shows that agricultural burning has an increasing trend in October. The agricultural fires in Anhui, Jiangsu, Henan, and Shandong provinces accounted for an average of approximately 59% of the total fires over the five years, and the largest annual average number of agricultural fires occurred in Anhui (Figure 9).

4.2. Uncertainty

In this paper, the accuracy of the results from fire monitoring is influenced by two factors. The first one is that there are some limitations associated with the use of the MODIS and the GlobeLand30-2010 data sets. The second is that the process of the GlobeLand30-2010 down sampling has a certain error in order to make the resolution of MOD14 and GlobeLand30-2010 data consistent.

The problem of the MODIS image resolution and the occurrence of many small fires falling below the MODIS detection limit for thermal anomalies led to some small agricultural fires not being recorded [30]. Moreover, a small number of MODIS images were not complete (Table 1), which resulted in an underestimation of agricultural fires. Weather conditions such as cloud cover and precipitation also affected the fire monitoring results.

The precision of the GlobeLand30-2010 data should also be considered as an important source of uncertainty. In our study, 2.7%, 3.1%, 2.4%, 2.7%, and 2.4% of the fire points were identified as falling on wetland and water bodies in 2010, 2011, 2012, 2013, and 2014, respectively, which is, of course, unrealistic. Based on using a multiple feature optimization method in pixel scale, the cultivated land type of GlobeLand30-2010 data was extracted [27]. Although the classification method has been taken into account in regards to the texture, spectrum, and phenological characteristics of the cultivated land as much as possible, the results of the classification have the phenomenon of fault and leakage. The accuracy of the land classes of GlobeLand30-2010 data is 83.06% [26], but when the land cover is misclassified, this may lead to false detection. The GlobeLand30-2010 data is divided into 10 categories, but land cover points of each category are not very detailed. Furthermore, the GlobeLand30 only has two phase data. Although the global land cover data of the GlobeLand30-2010 data has high accuracy and resolution in recent years, the cultivation areas in 2014 have change compared with 2010. In this article, the cropland data of GlobeLand30-2010 data was used from 2010 to 2014, which could impart an influence on the results from agricultural fires.

5. Conclusions

We used MOD14 images from 2010 to 2014 to analyze the distribution of fires in the main land cover types in China in accordance with the land cover classes of China that appear in the recently developed GlobeLand30-2010 data, According to GlobeLand30-2010 data classification results, we found that agricultural fires, artificial surface fires, forest fires, and grassland fires contributed to an

annual average of 95% of all the fires occurring in China, and that these fires represented the main biological fires that occurred during summers and autumns in China. In this study, agricultural burning was a significant contributor to the fire activity of China in the summer and autumn, accounting for 55%–64% of the total fires. The spatial distribution of the agricultural fires in China was quite similar over the five years, but the interannual numbers of agricultural fires showed certain differences. In this paper, we have provided a description of the space-time dynamic trends in agricultural burning across the seven geographic regions of China. The seasonal and interannual trends in agricultural fire activity were consistent with known regional agricultural practices. Extensive agricultural burning occurred in the Central and Eastern China regions during summer and autumn, which showed similar seasonality in their year-to-year agricultural fire activity. We also analyzed how the different crop planting/harvesting times and the weather conditions influenced fire activity. The results showed that agricultural burning was dependent on crop type and management practices.

We are now preparing a more detailed study of the fire activity of other land cover types, combined with an analysis of China's relevant policies in these various geographic areas of China.

Acknowledgments: The work described in the paper was substantially supported by the Shanghai Rising-Star Program (Project No. 15QA1403700), the International S&T Cooperation Program of China (Project No. 2015FDA11360), the National Natural Science Foundation of China (Project Nos. 41201426, 41325005, 41571407 and 41611130113), the National Basic Research Program of China—973 Program (Project No. 2012CB957701), and the Fundamental Research Funds for the Central Universities.

Author Contributions: Huan Xie and Li Du conceived the study, supervised the experiments, and edited the manuscript. The other co-authors contributed to the analysis, discussion, and manuscript editing. All the authors contributed significantly and participated sufficiently to take responsibility for this research. Moreover, all the authors are in agreement with the submitted and accepted versions of the publication.

Conflicts of Interest: The authors declare no conflict of interest.

References

1. Levine, J.S.; Cofer, W.R.; Cahoon, D.R.; Winstead, E.L. Biomass burning: A driver for global change. *Environ. Sci. Technol.* **1995**. [CrossRef]
2. Reisen, F.; Meyer, C.P.; Keywood, M.D. Impact of biomass burning sources on seasonal aerosol air quality. *Atmos. Environ.* **2013**. [CrossRef]
3. Andreae, M.O.; Merlet, P. Emission of trace gases and aerosols from biomass burning. *Glob. Biogeochem. Cy.* **2001**. [CrossRef]
4. Korontzi, S.; McCarty, J.; Loboda, T.; Kumar, S.; Justice, C. Global distribution of agricultural fires in croplands from 3 years of Moderate Resolution Imaging Spectroradiometer (MODIS) data. *Glob. Biogeochem. Cy.* **2006**. [CrossRef]
5. Cao, G.L.; Zhang, X.; Zheng, F. Inventory of black carbon and organic carbon emissions from China. *Atmos. Environ.* **2006**. [CrossRef]
6. McCarty, J.L.; Korontzi, S.; Justice, C.O.; Loboda, T. The spatial and temporal distribution of crop residue burning in the contiguous United States. *Sci. Total Environ.* **2009**, *407*, 5701–5712. [CrossRef] [PubMed]
7. Singh, R.P.; Kaskaoutis, D.G. Crop residue burning: a threat to south Asian air quality. *Eos Trans. Am. Geophys. Union.* **2014**. [CrossRef]
8. Roy, D.P.; Boschetti, L.; Justice, C.O.; Ju, J. The collection 5 MODIS burned area product—Global evaluation by comparison with the MODIS active fire product. *Remote Sens. Environ.* **2008**, *112*, 3690–3707. [CrossRef]
9. Xia, X.; Zong, X.; Sun, L. Exceptionally active agricultural fire season in mid-eastern China in June 2012 and its impact on the atmospheric environment. *J. Geophys. Res. Atmos.* **2013**, *118*, 9889–9900. [CrossRef]
10. Justice, C.O.; Giglio, L.; Korontzi, S.; Owens, J.; Morisette, J.T.; Roy, D.P. The MODIS fire products. *Remote Sens. Environ.* **2002**. [CrossRef]
11. Csiszar, I.; Justice, C.O.; Mcguire, A.D.; Cochrane, M.A.; Roy, D.P.; Brown, F.; Conard, S.G.; Frost, P.G.H.; Giglio, L.; Elvidge, C.; et al. Land use and fires. In *Land Change Science: Observing, Monitoring, and Understanding Trajectories of Change on the Earth's Surface*; Gutman, G., Janetos, A.C., Justice, C.O., Moran, E.F., Mustard, J.F., Rindfuss, R.R., Skole, D., Turner, B.L., Cochrane, M.A., Eds.; Kluwer Academic Publishers: Boston, MA, USA, 2004; Volume 6, pp. 329–350.

12. Dwyer, E.; Pinnock, S.; Gregoire, J.M.; Pereira, J.M.C. Global spatial and temporal distribution of vegetation fires as determined from satellite observations. *Int. J. Remote Sens.* **2000**, *21*, 1289–1302. [CrossRef]
13. Witte, J.C.; Douglass, A.R.; da Silva, A.; Torres, O.; Levy, R.; Duncan, B.N. NASA A-Train and Terra observations of the 2010 Russian wildfires. *Atmos. Chem. Phys.* **2011**, *11*, 9287–9301. [CrossRef]
14. Zha, S.; Zhang, S.; Cheng, T.; Chen, J.; Huang, G.; Li, X.; Wang, Q. Agricultural fires and their potential impacts on regional air quality over China. *Aerosol Air Qual. Res.* **2013**, *13*, 992–1001. [CrossRef]
15. Kaufman, Y.J.; Justice, C.O.; Flynn, L.P.; Kendall, J.D.; Prins, E.M.; Giglio, L.; Ward, D.E.; Menzel, W.P.; Setzer, A.W. Potential global fire monitoring from EOS-MODIS. *J. Geophys. Res.* **1998**, *103*, 32215–32238. [CrossRef]
16. Giglio, L.; Csiszar, I.; Justice, C.O. Global distribution and seasonality of active fires as observed with the Terra and Aqua MODIS sensors. *J. Geophys. Res.* **2006**, *111*, 2156–2202. [CrossRef]
17. McCarty, J.L.; Justice, C.O.; Korontzi, S. Agricultural burning in the Southeastern United States detected by MODIS. *Remote Sens. Environ.* **2007**, *108*, 151–162. [CrossRef]
18. Tulbure, M.G.; Wimberly, M.C.; Roy, D.P.; Henebry, G.M. Spatial and temporal heterogeneity of agricultural fires in the central United States in relation to land cover and land use. *Landscape Ecol.* **2011**. [CrossRef]
19. Liu, M.X.; Song, Y.; Yao, H.; Kang, Y.N.; Li, M.M.; Huang, X.; Hu, M. Estimating emissions from agricultural fires in the North China Plain based on MODIS fire radiative power. *Atmos. Environ.* **2015**. [CrossRef]
20. Huang, X.; Li, M.; Li, J.; Song, Y. A high-resolution emission inventory of crop burning in fields in China based on MODIS thermal anomalies/fire products. *Atmos. Environ.* **2012**, *50*, 9–15. [CrossRef]
21. Huang, X.; Song, Y.; Li, M.; Li, J.; Zhu, T. Harvest season, high polluted season in east China. *Environ. Res. Lett.* **2012**. [CrossRef]
22. Streets, D.G.; Bond, T.C.; Carmichael, G.R.; Fernandes, S.D.; Fu, Q.; He, D.; Klimont, Z.; Nelson, S.M.; Tsai, N.Y.; Wang, M.Q.; Woo, J.H.; Yarber, K.F. An inventory of gaseous and primary aerosol emissions in Asia in the year 2000. *J. Geophys. Res.* 2003. [CrossRef]
23. Justice, C.O.; Townshend, J.R.G.; Vermote, E.F.; Masuoka, E.; Wolfe, R.E.; Saleous, N.; Roy, D.P. An overview of MODIS land data processing and product status. *Remote Sens. Environ.* **2002**, *83*, 3–5. [CrossRef]
24. Giglio, L. *MODIS Collection 5 Active Fire Product User's Guide Version 2.4*; Science Systems and Applications: Lanham, MD, USA, 2010.
25. National Geomatics Center of China (NGCC). Available online: http://ngcc.sbsm.gov.cn/article/en/ps/mp/201302/20130200001694.shtml (accessed on 8 June 2016).
26. Chen, J.; Liao, A.P.; Cao, X.; Chen, L.J.; Chen, X.H.; He, C.Y.; Han, G.; Peng, S.; Lu, M.; Zhang, W.W.; et al. Global land cover mapping at 30 m resolution: A POK-based operational approach. *ISPRS J. Photogramm. Remote Sens.* **2015**. [CrossRef]
27. Liu, J.Y. Analysis of Land Cover Change in Northwest China and Its Driving Factors Based on Globeland30. Master's Thesis, Southwest Jiaotong University, Chengdu, China, 2015. (In Chinese).
28. Ministry of Agriculture of the People's Republic of China (MOA). Database of Farming Season, 2010–2014. Available online: http://www.moa.gov.cn/ (accessed on 15 April 2016). (In Chinese)
29. National Bureau of Statistics of the People's Republic of China (NBSC). Agriculture in: China Statistical Yearbook 2010–2015. Available online: http://www.stats.gov.cn/tjsj/ndsj/ (accessed on 14 April 2016). (In Chinese)
30. Morisette, J.T.; Giglio, L.; Csiszar, I.; Setzer, A.; Schroeder, W.; Morton, D.; Justice, C.O. Validation of MODIS active fire detection products derived from two algorithms. *Earth Interact.* **2005**, *9*, 1–25. [CrossRef]